Universität zu Köln

Mathematisch-Naturwisenschaftliche Fakultät
1. Physikalisches Institut

Bachelor Thesis

A Multiparticle Simulation of MRK 231 as a Triple Galactic Interaction

Submitted by:

Micah Ryan Bowles

Matrikelnummer 5622352

First Referee	Prof. Dr. Andreas Eckart
Second Referee	Prof. Dr. Lukas Labadie
Supervisor	Prof. Dr. Andreas Eckart

November 16^{th} 2018

Abstract

MRK 231 is the closest known quasar at approximately 600 Mly from earth and is well known to have double tails protruding from it. This thesis explores a formation model which creates a third much dimmer (less massive) tail which is clearly visible when the images of MRK 231 are viewed with care. We create a formation model of MRK 231 and compare the results of this model to original images of the system. We use an N-body predictor-corrector simulation method which is easily implemented and can create clear structures with minimal computing costs which is ideal for our purposes. The model we create suggests that the structure of MRK 231 can form through a triple galactic merger and may even require an interaction such as this to help form its larger asymmetrical tails. We investigate the model dependent upper and lower mass bounds of our third (less massive) galaxy and find that these are quite fitting to any measurements we can make on the flux of the MRK 231 tails themselves.

Zusammenfassung

MRK 231 ist mit einer Entfernung von etwa 600 Mlyr der naheliegendste Quasar zur Erde und ist bekannt für seine markanten zwei herausragenden Arme. In dieser Arbeit wird eine mögliche Entstehungstheorie dessen erforscht, die sich insbesondere mit einem dunkleren, dritten Arm befasst, welcher erst bei genauerer Betrachtung von MRK 231 sichtbar wird. Dazu erzeugen wir ein Modell zu dessen Entstehung und vergleichen diese Resultate mit Observationen von MRK 231. Zur Simulation wird eine "N-body predictor-corrector"-Methode benutzt, welche sich durch eine relativ leichte Implementierung und einen geringen Rechenaufwand auszeichnet und sich damit für unsere Voraussetzungen als ideal erweist. Unsere Modellierung zeigt als potentiellen Ursprung der Struktur von MRK 231 das Zusammentreffen und Fusionieren dreier Galaxien und deutet darauf hin, dass die Asymmetrie der Arme nicht ohne eine derartige Interaktion nachvollziehbar ist. Wir untersuchen darauf aufbauend die vom Modell abhängige obere und untere Schranke der Masse der dritten, am wenigsten massiven Galaxie und entdecken, dass sich unsere Ergebnisse mit Messungen des Flusses aus dem Bereich der Arme des Systems in Einklang bringen lassen.

Acknowledgements

This thesis was made possible through research done by the following facilities.

This research has made use of the NASA/IPAC Extragalactic Database (NED), which is operated by the Jet Propulsion Laboratory, California Institute of Technology, under contract with the National Aeronautics and Space Administration.

This research has made use of the NASA/ IPAC Infrared Science Archive, which is operated by the Jet Propulsion Laboratory, California Institute of Technology, under contract with the National Aeronautics and Space Administration.

The Digitized Sky Survey was produced at the Space Telescope Science Institute under U.S. Government grant NAG W-2166. The images of these surveys are based on photographic data obtained using the Oschin Schmidt Telescope on Palomar Mountain and the UK Schmidt Telescope. The plates were processed into the present compressed digital form with the permission of these institutions.

The Second Palomar Observatory Sky Survey (POSS-II) was made by the California Institute of Technology with funds from the National Science Foundation, the National Aeronautics and Space Administration, the National Geographic Society, the Sloan Foundation, the Samuel Oschin Foundation, and the Eastman Kodak Corporation. The Oschin Schmidt Telescope is operated by the California Institute of Technology and Palomar Observatory.

The UK Schmidt Telescope was operated by the Royal Observatory Edinburgh, with funding from the UK Science and Engineering Research Council (later the UK Particle Physics and Astronomy Research Council), until 1988 June, and thereafter by the Anglo-Australian Observatory. The blue plates of the southern Sky Atlas and its Equatorial Extension (together known as the SERC-J), the near-IR plates (SERC-I), as well as the Equatorial Red (ER), and the Second Epoch [red] Survey (SES) were all taken with the UK Schmidt telescope at the AAO.

Contents

1 Introduction

Markarian 231 (hereafter MRK 231) contains the closest known quasar.[1] Its prominent double tails are the result of a galactic merger.

A third tail is also visible, although much dimmer and more diffuse (see figure 2). We expect this to be the result of a third galaxy interacting with the system during its formation. Through N-body simulations we can show that this triple tail structure can be produced by a simple triple galactic interaction.

Section 2 describes the fundamental ideas used in this paper. This includes information on MRK 231, the simulation method we use as well as the motivation behind our research and justification of our simplifications.

Section 3 presents the functional side of our program, our simulation's restrictions and some early successes of our simulation including reproducing double tail formation through a double galactic merger.

Section 4 presents our final results and compares these to the data collected on MRK 231 and a model dependent mass prediction.

We conclude our thesis with suggestions on research to come and improvements which could be made (see section 5).

[1] European Space Agency: http://sci.esa.int/jump.cfm?oid=42663 (2018-10)

2 Theoretical Background

The following will present some introductory concepts to the non-specialist. Cursory knowledge of these concepts is necessary to understand the methods and conclusions presented in this paper.

2.1 N-Body Problem

The N-body problem is the famous problem of trying to solve the equations of motion for N particles in a given field. In our case we consider the Newtonian gravitational field.

The two body problem is one where two point masses are considered in the gravitational potentials created by one another. One can show that the exact solution to this two body problem (see: Torsten Fließbach Mechanik, Lehrbuch zur Theoretischen Physik: chapter 17) in polar coordinates is:

$$r(\phi) = \frac{p}{1 + \epsilon \cos \phi}$$

With:

$$p = \frac{l^2}{\mu G m_1 m_2} \ , \ \epsilon = \sqrt{1 + \frac{2 E_{total} l^2}{\mu (G m_1 m_2)^2}}$$

Whereby μ is the reduced mass of the two bodies and l is the angular momentum of the body in question around the centre of mass.

There is no analytic solution to the N-body problem. We approximate all solutions using numerical methods to solve this problem as best we can. We can directly calculate the acceleration at a given time of particle i in an N-body problem by summing over the force created by the gravitational potential of each of the other particles j:

$$\frac{\mathbf{F}_i}{m_i} = \ddot{\mathbf{r}}_i = G \sum_{j \neq i} \frac{m_j \mathbf{r}_{ij}}{|\mathbf{r}_{ij}|^3} \tag{1}$$

This is the basic calculation which our simulation relies on. See section 2.5.1 for more details on the calculations made.

2.2 Markarian 231

In 1963 Benjamin Markarian brought attention to a set of galaxies that have nuclei with abnormaly high amounts of ultraviolet emissions. Beginning in 1967 listings of Markarian

galaxies were published, the first being Markarian, 1967. In the first publication only 70 galaxies were listed. The final Markarian galaxies numbered 1500 in 1981. Since then additional objects matching these conditions have been discovered, specifically they were discovered by the first (Markarian et al., 1989) and second Byurakan surveys (Stepanian, 2005) which looked at dimmer objects. The objects catalogued under 201 - 302 were first published as a list in Markaryan, 1969.

MRK 231, depicted in figure 1 as seen in the night sky, was discovered in 1969 and contains the closest known quasar to earth at approximately 600 Mlyr[2]. It has two prominent tidal tails and a "disturbed shape". Having been classified as an Ultra Luminous Infrared Galaxy (ULIRG) with a very compact nucleus and is singular within the Markarian sample due to it having a powerful quasar at its centre.[3]

Recently sources have stated that MRK 231 has a binary black hole at its centre (Yan et al., 2015) but this has also been called into question (Leighly et al., 2016). The coordinates of MRK 231 are presented in table 1.

The reason we show significant interest in this system is due to figure 2 and the implications which go along with the visualisation of a third tail by carefully examining images of the system.

Units	**Longitude**	**Latitude**
Decimal Degrees	194.059308	56.873677
Sexigesimal	12h56m14.2339s	+56d52m25.237s

Table 1: Equitorial J2000.0 Coordinates of MRK 231 (Ma et al., 1998)

2.3 Motivation: Toomre & Toomre

In Alar Toomre and Juri Toomre's 1972 paper titled "Galactic Bridges and Tails" we see many close encounters which are generously simplified but still yield very clear results.

The calculations made by Toomre & Toomre were only three body calculations between the two central masses and each of the particles in the disk respectively. These extremely simplified simulations were able to demonstrate that bridges and tails can be seen to form through tidal kinematic interactions.

The demonstration of seemingly "crossed" tails of NGC 4038/9 (Toomre & Toomre pg. 658-660) is of special interest to us since the two prominent tails of MRK 231 seem

[2]European Space Agency: http://sci.esa.int/jump.cfm?oid=42663 (2018-10)
[3]ESA: http://sci.esa.int/jump.cfm?oid=42663 (2018-10)

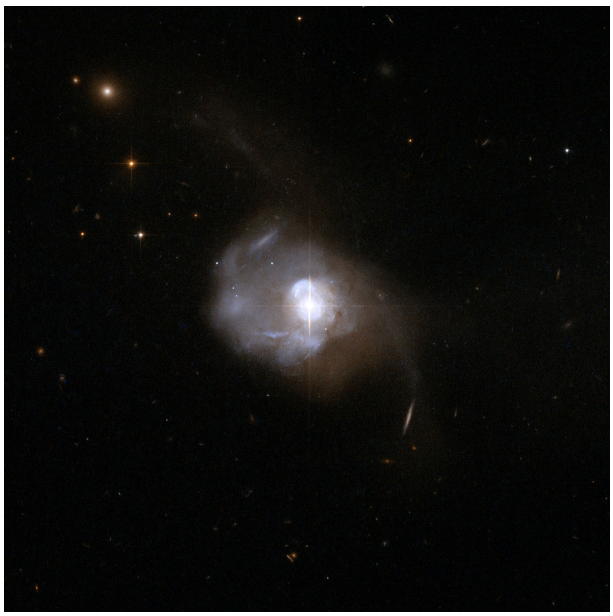

Figure 1: MRK 231 as taken by Hubble in 2008. (http://sci.esa.int/hubble/42663-markarian-231/)

to be crossed in a similar fashion (an image of which can be seen in figure 4). We can use this as a foundation to add a third smaller galaxy to create the third tail.

Due to the simplified calculations made in Toomre & Toomre, the complexity of the systems which could be modelled was extremely limited. We improve on this by using N-body calculations. This is not the most modern method but will show itself to be a simple and effective system to create our model.

2.4 Double Tails

Double tails are a galactic structure which can appear when two galaxies have a close encounter. A detailed exploration of how they can be formed is found in A. Toomre and J. Toomre, 1972, where on pg. 633 a notation style is set for the position of a galaxy in relation to the orbital plane. Figure 3 shows the respective angles which are used to describe the starting positions of such an interaction.

This nomenclature was used in the same Toomre & Toomre paper to create a simple model of NGC 4038/9. In section IV of the Toomre paper we see an analysis of the tidal processes from which double tail structures can emerge. Since our MRK 231 system clearly has "double crossed tails" similar to those of NGC 4038/9 (fig. 4) we will make special note of the starting conditions used in the simulation of this system.

The caption of Toomre & Toomre's (1972) figure 23 states these conditions as follows:

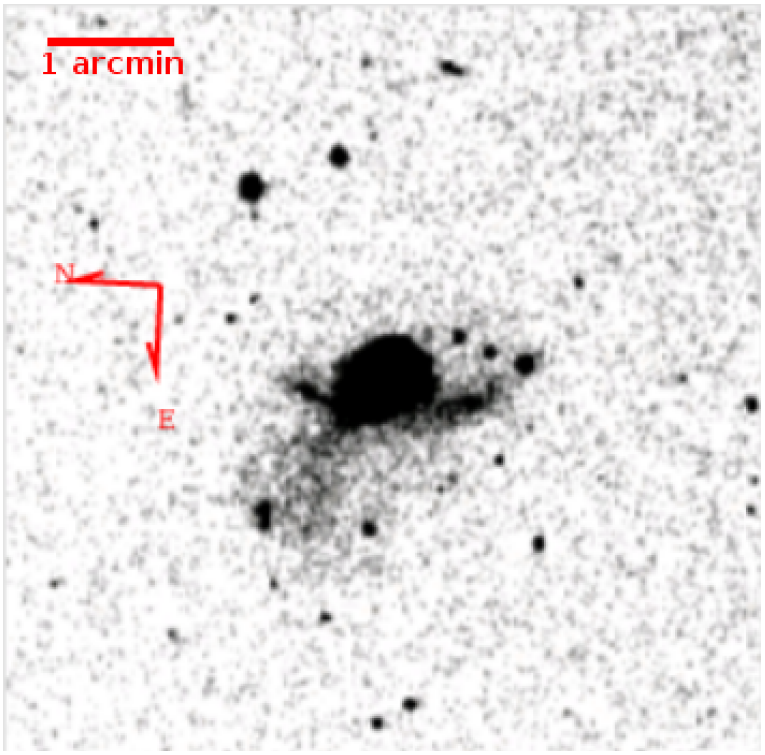

Figure 2: DSS POSS-II UK Schmidt Telescope (blue 1993): IRSA finder chart image of MRK 231 linearly stretched with upper and lower sigma bounds of 0 and 10 respectively.

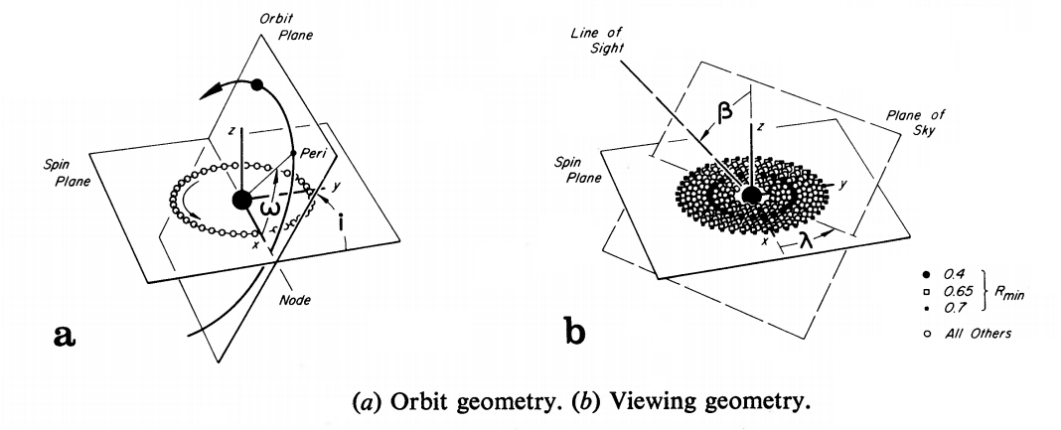

(*a*) Orbit geometry. (*b*) Viewing geometry.

Figure 3: Depiction of the notation defined by Toomre & Toomre (fig. 6 in the original 1972 paper)

"Here two identical disks of radius $0.75R_{min}$ suffered an $e \approx 0.5$ encounter with orbit angles $i_8 = i_9 = 60°$ and $w_8 = w_9 = -30°$ that appeared the same to both [...] The viewing time is $t = 15$, or slightly past apocenter." These are the starting conditions which we use to begin our search for a double tail system similar to the strong tails of MRK 231 before we initialise a third galaxy.

Figure 4: RGB image of The Antennae Galaxies NGC 4038 and NGC 4039. Data from the Liverpool Telescope, a 2 m RC telescope on La Palma. Processed by Göran Nilsson. Exposures: 58 x 60s = 1 hour.

2.5 Simulation Method

Simulation methods can vary greatly. More modern cosmic simulations are usually hydrodynamic simulations. These sorts of simulations would be too complicated for this thesis.

The simulations made by Toomre & Toomre (1972) are simple three body force calculations and have their restrictions due to these simplifications. The method used here is not as simplified as Toomre & Toomre used, but is still quite simplified and has restrictions of its own.

We are interested in the Newtonian N-body problem. Our predictor-corrector method has been used primarily due to its simplicity and is detailed in section 2.5.1.

2.5.1 Predictor-Corrector Method

This description and implementation of the predictor-corrector method we use is strongly aligned to the more detailed description in Aarseth, 2003 chapter 2.

The forces acting on particles subject only to gravitational forces vary smoothly throughout time. This allows for a polynomial fit of the force (acceleration) at earlier times as to predict the force at a time $t_0 + \Delta t$. We use the following equation to extrapolate the force at that 'future' time using four known forces at previous times (t_1, t_2, t_3) and the t_0 as the 'current' time where $i < j \Leftrightarrow t_i < t_j$.

$$\mathbf{F}_t = \{[(\mathbf{D}^4(t - t_3) + \mathbf{D}^3)(t - t_2) + \mathbf{D}^2](t - t_1) + \mathbf{D}^1\}(t - t_0) + \mathbf{F}_0$$

whereby the divided differences ($\mathbf{D}^k$) are

$$\mathbf{D}^k[t_0, t_k] = \frac{\mathbf{D}^{k-1}[t_0, t_{k-1}] - \mathbf{D}^{k-1}[t_1, t_k]}{t_0 - t_k} \quad , \ (k = 1, 2, 3)$$

Converting from the force polynomials to a Taylor series, we can calculate the first four orders of the force polynomial using the divided differences. We define $t'_k := t_0 + t_k$.

$$\begin{aligned}
\mathbf{F}^{(1)} &= [(\mathbf{D}^4 t'_3 + \mathbf{D}^3)t'_2 + \mathbf{D}^2]t'_1\mathbf{D}^1 \\
\mathbf{F}^{(2)} &= 2![\mathbf{D}^4(t'_1t'_2 + t'_2t'_3 + t'_1t'_3) + \mathbf{D}^3(t'_1 + t'^2) + \mathbf{D}^2] \\
\mathbf{F}^{(3)} &= 3![\mathbf{D}^4(t'_1 + t'_2 + t'_3) + \mathbf{D}^3] \\
\mathbf{F}^{(4)} &= 4!\mathbf{D}^4
\end{aligned} \tag{2}$$

The terms involving $\mathbf{D}^4$ are only included in the prediction steps where the force at

$t_0 + \Delta t$ is calculated. Usually the force calculations will be to the third force order and of time $t = t_0$.

To initialise the system of N particles we define $\mathbf{R} = \mathbf{r}_i - \mathbf{r_j}$ and $\mathbf{V} = \mathbf{v}_i - \mathbf{v}_j$. We calculate the force derivatives by differentiating equation 1. This leads to equations 3.

$$\begin{aligned}
\mathbf{F}_{ij} &= -m_j\mathbf{R}/R^3 \\
\mathbf{F}^{(1)}_{ij} &= -m_j\mathbf{V}/R^3 - 3a\mathbf{F}_ij \\
\mathbf{F}^{(2)}_{ij} &= -m_j(\mathbf{F}_i - \mathbf{F}_j)/R^3 - 6a\mathbf{F}^{(1)}_{ij} - 3b\mathbf{F}_ij \\
\mathbf{F}^{(3)}_{ij} &= -m_j(\mathbf{F}^{(1)}_i - \mathbf{F}^{(1)}_j)/R^3 - 9a\mathbf{F}^{(2)}_{ij} - 9b\mathbf{F}^{(1)}_{ij} - 3c\mathbf{F}_{ij}
\end{aligned} \tag{3}$$

where

$$\begin{aligned}
a &= \mathbf{R}\cdot\mathbf{V}/R^2 \\
b &= \left(\frac{V}{R}\right)^2 + \frac{\mathbf{R}\cdot(\mathbf{F}_i - \mathbf{F}_j)}{R^2} + a^2 \\
c &= \frac{3\mathbf{V}\cdot(\mathbf{F}_i - \mathbf{F}_j)}{R^2} + \frac{\mathbf{R}\cdot(\mathbf{F}^{(1)}_i - \mathbf{F}^{(1)}_j)}{R^2} + a(3b - 4a^2)
\end{aligned}$$

For each particle i the force and force derivatives can be calculated by summing over all $j \in \{[1, \ldots, N]\backslash i\} \subset \mathbb{N}$.

The remaining terms we need for our initialisation are the starting values for the divided differences and the time-steps needed to calculate these. The time steps are initialised backwards from $t_0 = 0$ such that $t_k = -k\Delta t_i$, $(k = 1, 2, 3)$. The time step is calculated the same for both the initialisation and the iteration:

$$\Delta t_i^2 = \frac{\eta(|\mathbf{F}||\mathbf{F}^{(2)}| + |\mathbf{F}^{(1)}|^2)}{|\mathbf{F}^{(1)}||\mathbf{F}^{(3)}| + |\mathbf{F}^{(2)}|^2} \tag{4}$$

The initial divided differences are calculated as:

$$\begin{aligned}
\mathbf{D}^1 &= (\frac{1}{6}\mathbf{F}^{(3)}t'_1 - \frac{1}{2}\mathbf{F}^{(2)})t'_1 + \mathbf{F}^{(1)} \\
\mathbf{D}^2 &= -\frac{1}{6}\mathbf{F}^{(3)}(t'_1 + t'_2) + \frac{1}{2}\mathbf{F}^{(2)} \\
\mathbf{D}^3 &= \frac{1}{6}\mathbf{F}^{(3)}
\end{aligned}$$

We make use of a Plummer softening parameter ϵ. We include this factor in all R terms in the denominators of equations (3) to reduce the effect of close encounters. We are therefore actually dealing with a potential in the form of:

$$\Phi = \frac{-m}{(R^2 + \epsilon^2)^{1/2}}$$

The integration loop begins by determining the next particle, i, to be advanced; i. e. the particle with the smallest value of $t_i + \Delta t_i$ (see: operation 3 of algorithm 1).

To output data we set a constant time step δt after which time we wish to output our data; i. e. every δt time units we will store the system's data. The n^{th} data set is stored when the global time (operation 4 of algorithm 1) satisfies $t > n\,\delta t$. We make third order predictions of the position and velocity of the particles, using the time difference between each particle's local time and the output time: $\tilde{t} = t_i - n\,\delta t$.

Algorithm 1 Modified from Aarseth, 2003

1: Initialise the system.
2: Store current data if: $t > n\,\delta t$
3: Determine the next particle: $i = \min_j\{t_j + \Delta t_j\}$
4: Set the new global time: $t = t_i + \Delta t_i$
5: Predict all coordinates $\mathbf{r}_j$ to order $\mathbf{F}^{(1)}$ (stored as $\mathbf{r}_t$)
6: Form $\mathbf{F}^{(2)}$ by the second equation of equations (2)
7: Improve $\mathbf{r}_i$ and predict $\mathbf{v}_i$ to order $\mathbf{F}^{(3)}$
8: Obtain the new force $\mathbf{F}_i$
9: Update the times t_k and differences $\mathbf{D}^k$
10: Apply the corrector $\mathbf{D}^4$ to $\mathbf{r}_i$ and $\mathbf{v}_i$
11: Specify the new time-step Δt_i
12: End program if stopping conditions have been fulfilled
13: Repeat from operation 2.

When we output the values, we use the following $\mathbf{F}^{(3)}$ order integration to determine the position and velocity of each particle at time $t = n\,\delta t$.

$$\mathbf{r}_j = \frac{1}{120}\mathbf{F}^{(3)}\,\tilde{t}_j{}^5 + \frac{1}{24}\mathbf{F}^{(2)}\,\tilde{t}_j{}^4 + \frac{1}{6}\mathbf{F}^{(1)}\,\tilde{t}_j{}^3 + \frac{1}{2}\mathbf{F}\,\tilde{t}_j{}^2 + \mathbf{v}_0\,\tilde{t}_j + \mathbf{r}_0$$
$$\mathbf{v}_j = \frac{1}{24}\mathbf{F}^{(3)}\,\tilde{t}_j{}^4 + \frac{1}{6}\mathbf{F}^{(2)}\,\tilde{t}_j{}^3 + \frac{1}{2}\mathbf{F}^{(1)}\,\tilde{t}_j{}^2 + \mathbf{F}\,\tilde{t}_j + \mathbf{v}_0$$

To get an idea of the precision of the simulation, we observe how well energy is conserved by calculating the energy of the system at the output times. This is done by

summing over the kinetic energy of each particle and summing over the potential energy of each particle (eqn. 5).

$$\begin{aligned} E_{kin} &= \sum_{i=1}^{N} \frac{1}{2} m_i |\mathbf{v}_i|^2 \\ E_{pot} &= -\sum_{i=1}^{N} \sum_{j>i}^{N} \frac{G m_i m_j}{|\mathbf{r}_i - \mathbf{r}_j|} \\ E_{total} &= E_{kin} + E_{pot} \end{aligned} \tag{5}$$

Each particle will need to have 31 variables assigned to it: m, $\mathbf{r}_0$, $\mathbf{r}_t$, $\mathbf{v}_0$, $\mathbf{F}$, $\mathbf{F}^{(1)}$, $\mathbf{D}^1$, $\mathbf{D}^2$, $\mathbf{D}^3$, Δt, t_0, t_1, t_1, t_2 and t_3. We define the variables used in our implementation in greater detail in section 3.1.1.

2.5.2 Various Galactic N-Body Simulations

N-body simulations are used for particular problems. Small galaxy groups and clusters are ideal subjects for N-body simulations, assuming one can treat close encounters using a softened potential.

Historically, N-body integration simulations, such as our predictor-corrector method, have been used to investigate a wide variety of problems. Aarseth, 2003 chapter 16 presents some of the research into galaxies using similar N-body methods. Aarseth states: "All such problems are characterized by the employment of a small softening of the potential which reduces the effect of close encounters" (pg. 297).

Subjects which have been studied include tidal disruptions of dwarf spheroid galaxies orbiting the Milky Way (Oh, Lin, and Aarseth, 1995). Stronger interactions generally lead to mergers. This is the situation we expect for MRK 231 whose structure implies a strong interaction due to the the two primary tails protruding from the central galactic body.

Binary black holes have been of particular interest to researchers and have led to simulations of various galactic interactions where the binary black hole is replaced by a merged central black hole. This would be the natural end of a binary black hole system as we have observed in the past, although the mechanics of this system are not fully understood, as exemplified by the final parsec problem (Milosavljević and Merritt, 2003). Our simulation does not merge the binary black hole at its centre. This is a relatively small structural concession in comparison to not considering the central molecular cloud.

3 Simulation

We expect there to be multiple different starting conditions which would lead to similar results, especially in regards to the multitude of viewing angles and viewing times. To create a system that mimics the structure of MRK 231, we initialise two galaxies in such a way as to create a double tail system and then initialise a third smaller galaxy passing through or near the two larger galaxies. To test these expectations we must first verify our system can create reliable results.

In this section we will expand on the initial conditions of our simulation, the limitations of our program and the restrictions we place upon ourselves to maintain the integrity of our results. To verify our system works we display the results of a simple double tail interaction in section 3.4.

3.1 Implementation

The three main parts of the program were implemented in three different files.

In the first file starting conditions (defined in section 3.1.1) are entered and final data is received. The final data is saved and plotted as a 3D graph. We use a slider to improve our intuitive understanding of the system's motion as well as to better display our results. All sliders were edited out of final figures for aesthetic reasons. This file was implemented in python for ease of plotting and greater legibility of the input data.

The second file is where the calculations outlined in section 2.5.1 were carried out in Cython. Cython was used due to the simple integration into python with the added benefit of being compiled into C and therefore running with C-like performance. In this file the input data is processed, the third file is called and the simulation method outlined in section 2.5.1 is run. The data which is stored during operation 4 of algorithm 1 is appended to NumPy arrays and passed back to the first file for plotting.

For galactic simulations data is passed from the second file to a third where the galactic structure is calculated. This file outputs the starting position of each particle as well as the velocity based off of its mass, its position in the galaxy and its velocity factor set in the starting conditions.

3.1.1 Starting Conditions

The nomenclature used by A. Toomre and J. Toomre, 1972 and depicted in figure 3 is perfectly suited, and commonly used, for double galactic interactions. For triple galactic interactions, there are too many degrees of freedom to solely rely on this. Therefore we

will introduce the simulation's starting conditions, which determine the 7 degrees of freedom of each of the particles in the simulation ($\mathbf{r}_i$, $\mathbf{v}_i$, m_i).

Instead of initialising each point individually (which would amount to $7 \cdot 3 \cdot 31 = 651$ individual data entries for the final simulation: 7 for each of the 31 particles in each of the 3 galaxies) we use twelve parameters to set the starting conditions of a system. These variables are listed below and include: η, ϵ, number of galaxies, N, outer radius, central mass, galactic mass ratios, velocity factors, rotations, translations and velocity transformations. We set these values in the first file and the structure defining calculations are primarily carried out in the third file (as stated in sect. 3.1). Each of the variables is listed with their variable name in brackets under which they can be initialised.

Output time step (deltat)

This is the time interval at which the simulation's data is saved to be for output at a later time (δt in sect. 2.5.1). We set this value to 1 Myr as this provides a smooth progression of the motion of our galaxies without creating excessively large data sets.

η (eta)

This is an accuracy parameter of each particles individual time-step as defined by equation 4 in section 2.5.1. This value is the same throughout all of our simulations and is set at 10^{-6}. There is no size limit set by the program for η or for how small the output time step can be. However, η should be proportionately much smaller than the output time steps (see above) otherwise the output data can be calculated incorrectly. This is because η determines the size of the individual time-steps of the particles, and if these steps exceed the size of the output time-steps, then the program will eventually be prompted to output a time t_n when a particle exceeds t_{n+1}. As it only outputs one time no matter how many thresholds are surpassed the $\tilde{t}$ of section 2.5.1 can become quite large. This error can then cascade as each particle moved can exceed at least 1 new time threshold without having the previous times output accurately. This can result in extremely misleading output data which seems normal at small output times, but can result in odd behaviour such as seemingly reversed motion.

ϵ^2 (eps2)

This is the Plummer constant outlined in section 2.5.1. It is also called a softening parameter, as it softens close encounters. This value is the same throughout all of our simulations and is equal to $10^{-2}\,pc$.

Step limit (stepscrit)

This is a stopping condition for our programme, which it checks against each time it outputs data - operation 2 of algorithm 1. If the total number of steps (loop iterations) of the run exceed this value, then the loop will break and the simulation will output the stored data. We primarily use a time limit (tcrit: see below) instead of a step limit as a conditional break, as the program's run time is not of a primary concern when only considering the first 1000 Myr. We therefore (mostly) have set this value to greater than 10^7 steps for our purposes.

Time limit (tcrit)

The same conditional check of the step limit is made of the time limit. We output data after the global time exceeds the time limit. This is a more practical way to control when the loops should end and output our data as we generally do not need data for $t > 1000$ Myr. It can be prudent to set this value to just above the time you would like to have output, as this will restrict processing time to the values you wish to consider.

Number of Galaxies (NumberOfGalaxies)

This is the number of galaxies being initialised. Value must be 1, 2 or 3.

Number of rings and particles (N)

This one dimensional array defines the number of particles in each of the galaxies. The length determines how many rings there are in each of the galaxies with the Cartesian position of each of the particles determined as described in section 3.2. The convention is to list the rings in order of decreasing number of particles (e. g. $[20, 10]$).

Outer Radius (radius)

This sets the radius of the first value of N (i. e. N[0]). The radius of the other rings are at radial values outlined in section 3.2.

Central Mass (BHMass)

Sets the mass of the centre of each galaxy. This also defines the mass of the rings, as the sum of the mass of the rings is equal to the mass of the centre of their respective galaxy. The value entered is in $M_\odot$

Galactic Mass Ratios (GalaxyMassRatios)

This one dimensional array, of length three, defines what factor the central mass is scaled by to set the final mass of each of the respective galaxies; i. e. $[1, 1, 0.5]$ would make galaxies 1 & 2 full mass but the third galaxy would be initialised with half mass. If the number of galaxies is less than 3 then the first and/or second mass ratios are used.

Velocity Factors (velFactor)

This two dimensional array with dimensions (3, length of N) sets a scaling factor for the speed of the individual rings of particles in galaxy 1, 2 and 3 respectively. The speed of a given particle in a ring is calculated by $v = v_{factor}\left(\frac{GM}{r_i}\right)^{1/2}$ this is based off of the approximation of orbital speed of a mass around a much larger mass. We found that the scaling of the speed was necessary even if using reduced mass. Some stable system's velocity factors are listed in table 2. These values are determined experimentally as the selection of which affects the stability of a galaxy (see sect. 3.3.2).

Rotations around x-Axis (xangle)

This one dimensional array of length 3 rotates all particles of a given galaxy (1, 2, or 3) by the set number of radians around the x-axis. We use the three dimensional rotation matrix to rotate the positions of the particles.

Rotations around y-Axis (yangle)

The second rotation matrix we apply rotates all particles around the y-axis (input radians).

Rotations around z-Axis (zangle)

Our final rotation matrix rotates all particles around the z-axis. If no further transformations were given, then all central masses would still be at $(0, 0, 0)$ as they were initialised in these positions.

Translations (r_transform)

This two dimensional array of size $(3, 3)$ contains the positional [x, y, z] translations of each of the galaxies; i. e. r_transform[0] is the [x, y, z] translation of the first galaxy etc. These translations are entered in kpc. For greater legibility the positional and velocity transformations are listed individually for each galaxy of a simulation in this paper, if none are listed for a galaxy, then the entered values are $[0, 0, 0]$.

Velocity Transformation (v_transform)

Using the same data structure as the translations, the velocity transformations provide Cartesian velocities for each of the galaxies. The values provided are in pc/Myr and are added to the velocity of each of the particles of the given galaxy, thus we refer to this as "group velocity" at later times.

Please note: All transformations (rotations, translations and velocity transformations) are performed in the same order as they are listed in.

3.2 Initial Structure

We primarily implement the structure we define for our galaxies in the third file (see section 3.1) where we implement a disc galaxy with an outer disc which has the same mass as the central bulge.

In our simulation we do not explicitly consider a molecular cloud in the inner part of our model galaxy. We omit this feature as it would not be a reasonable inclusion until a larger number of particles is considered. We approximate the mass distribution of the cloud through our central particle. This is one aspect in which our model differs from both reality and the ideal simulation. Aarseth [2003] states that the initial galactic models consisted of 124 equal-mass particles in the galactic cloud which orbit a small central mass with 125 particles stabilising the system in an outer ring. Even with 124 and 125 particles respectively, Aarseth notes that "the relevant time-scales are somewhat shorter" this is how the "slightly smaller particle number" is justified. As we are dealing with particle numbers N<100 for the entire system, we acknowledge this as an area for improvement for future models in regards to the structure of our galaxies.

To generate our galaxy-like structure we set the number of particles N, a radius for an outer ring and a mass of the entire galaxy (see section 3.1.1 for details on variables). The most common structure we use has an outer radius of 30 kpc, a mass of $2 \cdot 10^{11}\,\mathrm{M}_\odot$ and consists of 31 particles arranged as 20 particles in an outer ring and 10 in an inner ring (code input: $\mathrm{N}[i] = [20, 10]$) with an additional particle as a galactic centre.

The 20 outer particles are spaced equally in an outer ring of radius $R = 30$kpc and the 10 inner particles spaced equally in an inner ring at radius of $\frac{10}{20} \cdot 30\mathrm{kpc} = 15\mathrm{kpc}$, i. e. all particles have the same arc length separation to their respective 'left' and 'right' neighbours.

The mass of the galactic centre is equal to the mass of all other particles. In this galaxy, that means we have a galactic centre of mass $10^{11}\,\mathrm{M}_\odot$ and each particle of the rings has a mass of $\frac{1}{30}10^{11}\,\mathrm{M}_\odot = 3.\dot{3} \cdot 10^9\,\mathrm{M}_\odot$.

3.3 Limitations

Table 7.1 of Aarseth, 2003 (pg. 107) notes the "typical particle numbers for applications". We note that our total number of particles is within the range specified there.

$$3 < N_{total} < 100$$

To demonstrate the accuracy of our results we consider two different factors: the

energy and the stability of a galaxy without tidal forces.

3.3.1 Conservation of Energy

Firstly, we consider the total energy of the system throughout the duration of the simulation. The energy of a single galaxy which has been created to be stable (see section 3.3.2) is plotted in figure 5. One can see a significant accuracy loss after 5500 Myr. We consider this point an absolute break-point for the accuracy of our simulation. We will therefore not consider any values after this time.

For $t < 5500$Myr the largest energy difference we have amounts to $(1.5 \cdot 10^{-5})\%$. As a comparison, the maximal difference before a time t_{chaos} (see sect. 3.3.2) is $(4 \cdot 10^{-9})\%$. This is a time we define as never being surpassed in any of our considerations.

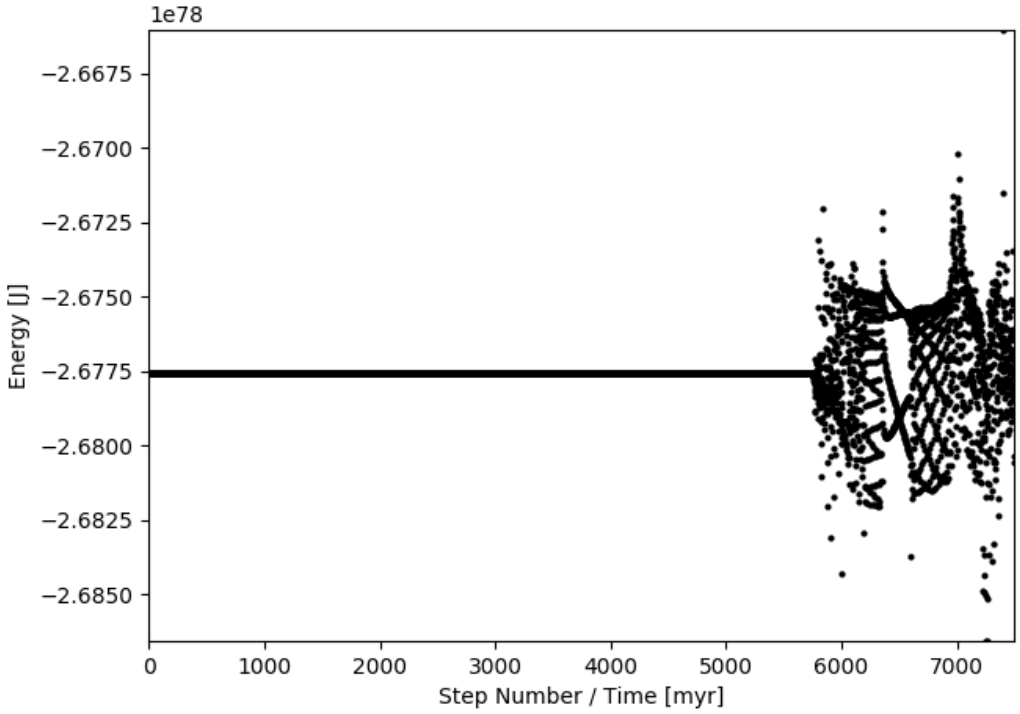

Figure 5: Time evolution of the energy of a single stable galaxy

3.3.2 Stable Galaxies

Finally, to be able to state with any certainty that the structure of the final simulation is due to galactic tidal interactions we consider the "life-expectancy" of our galaxy when void of tidal forces. We define stable galaxies which we use for our final simulation.

To do this, we define three times in the life cycle of a galaxy.

t_{start} is the time at which we initialise the system. $t_{start} = 0$ unless stated otherwise.

$t_{symmetry}$ is the time at which the galaxy first loses its initial structure. The galaxy maintains symmetry past this time.

t_{chaos} is the time at which the galaxy first loses its symmetry. Meaning, we cannot be certain that galactic superstructures arising after this time are due to tidal forces and not the seemingly chaotic motion of our galaxies.

To guarantee the integrity of our results we will refrain from surpassing t_{chaos} in our analysis.

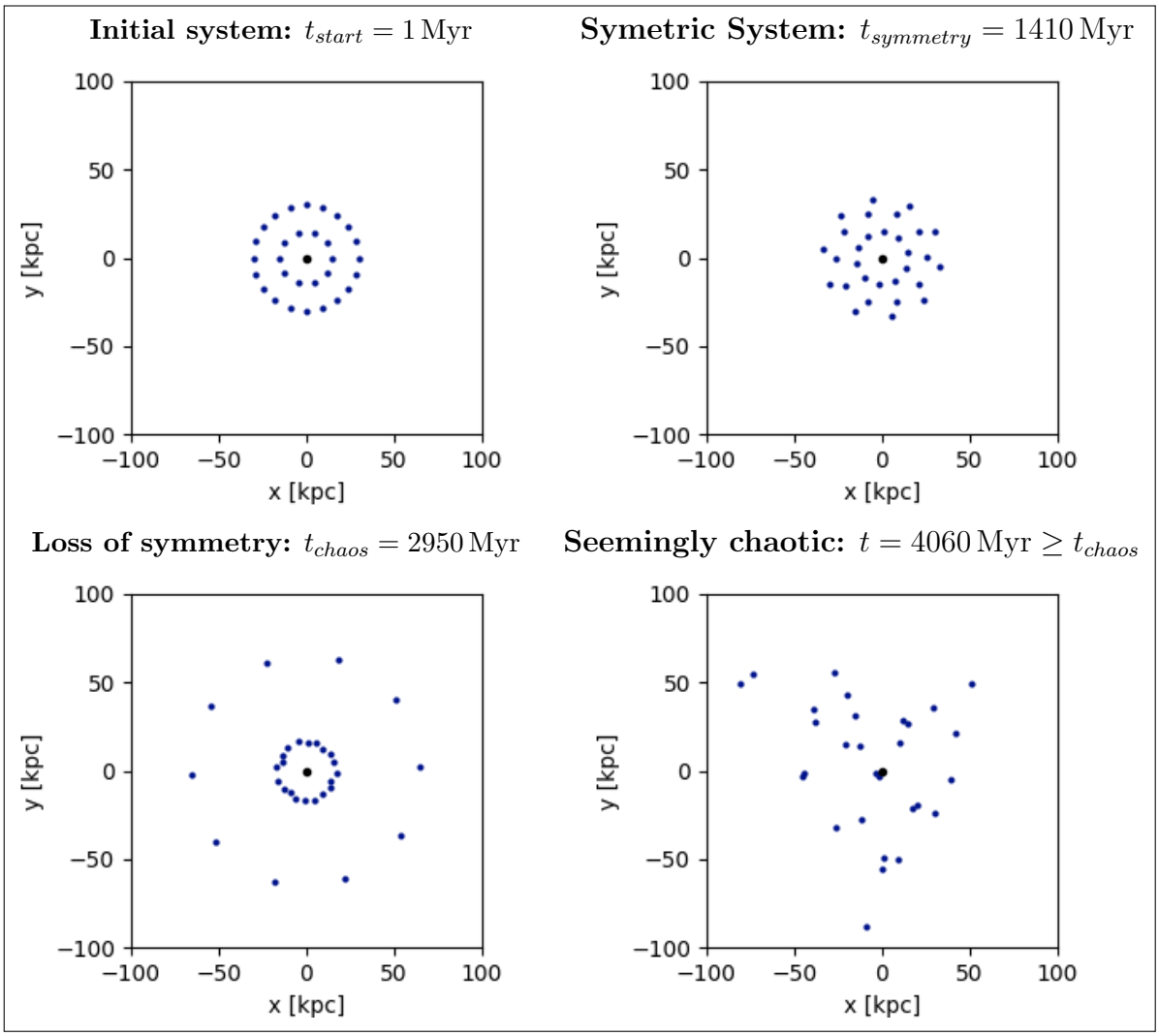

Figure 6: Progression of an initially stable galaxy. Note: before $t_{symmetry}$ the system is defined to be equivalent to a rotation of the galaxy at t_{start}.

Examples of starting conditions which lead to stable galaxies are listed in table 2.

N	Radius [kpc]	v_{factor}	Mass Ratio	$t_{symmetry}$ [Myr]	t_{chaos} [Myr]
[8]	10	[1.142]	1	n.a.	1210
[10]	10	[1.168]	1	n.a.	1090
[25]	10	[1.2]	1	930	960
[20]	10	[1.217]	1	460	510
[20]	30	[1.217]	1	2100	> 2200
[20, 10]	30	[1.32, 1.03]	1	1215	> 2900
[20, 10]	22.5	[1.32, 1.03]	1	775	1900
[20, 10]	22.5	[0.85, 0.665]	0.5	1150	> 2800
[20, 10]	22.5	[0.65, 0.5]	0.3	1700	> 3300
[20, 10]	22.5	[0.51,0.4]	0.2	1850	> 4500
[20, 10]	22.5	[0.35, 0.265]	0.1	2700	> 4500
[20, 10]	22.5	[0.258,0.194]	0.05	> 4900	> 8000

Table 2: Examples of stable galaxies and their respective collapse and chaos times. The central mass of each of these galaxies was initially set to $10^{11}\mathrm{M}_{\odot}$. We initialise a single xy-plane galaxy with a low z velocity to prevent the programme from encountering a 'div0' error when considering the central particle.

The time values listed as "n.a." (not applicable) were not able to be determined, as the evaluation seemed to produce only one shift from the original symmetry, this is most likely due to the fact that $t_{symmetry} \simeq t_{chaos}$ for those systems.

3.4 Double Tails

Demonstrating that our simulation can produce tidal tails, we initialise a system which should produce tidal tails according to A. Toomre and J. Toomre, 1972. To increase visibility of the structure this simulation was done with a single 20 particle ring on either galaxy (see table 2 for stability conditions). Figure 7 and 8 show us the system from two different angles, where we can clearly see double tails.

Table 3 contains the starting conditions required to initialise this system.

Condition	Value
N	[20]
Radius	$30\,kpc$
i: relative incline	$\pm 30°$
v_1 of galaxy 1	$60\,pc/Myr$
v_2 of galaxy 2	$-60\,pc/Myr$

Table 3: Double tail initialisation conditions. See table 2 for v_{factor} used and respective stable time periods.

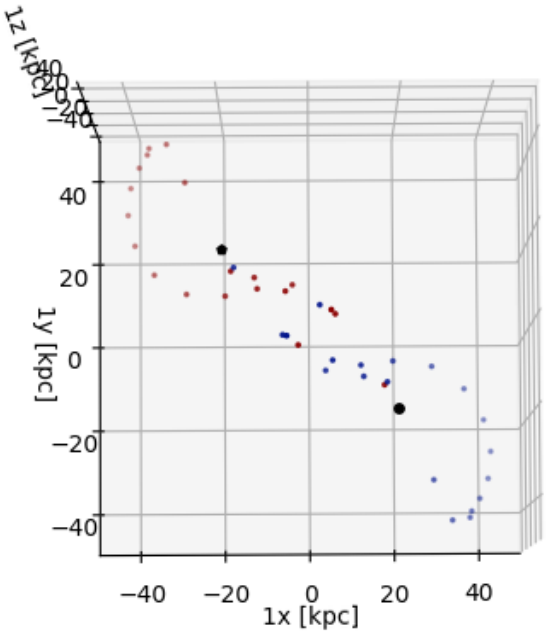

Figure 7: View of double tail system perpendicular to the xy-plane

3.5 Visualisation

Due to the low number of particles in our simulation, 31 particles per galaxy for a maximum of 93 in a given simulation, it is difficult to ascertain if a single particle is indicative of a larger structure or if it is a single outlying particle. For example if there is a close encounter in a simulation with 93 particles and one of the particles is elevated out of the structure, we may not be able to determine whether or not this would be a single occurrence or if we can expect to see a large number of particles clustered here if we were to arrange a larger simulation.

To minimise any confusion around these abnormal particles, and to gain a better visual understanding of the structures involved, we run the simulation 15 times with minimal alterations to the starting conditions and overlap the resulting data to produce a single image with a total of 1395 plotted points where any single particle will not be of much interest.

In our final system we initialise with 20 outer particles the angular separation of two outer particles is $\frac{\pi}{10}$ (with the centre of the galaxy as the origin). We rotate all galaxies around its rotation axis by five different angles: $\Delta\theta = \left\{0,\ \frac{\pi}{50},\ \frac{2\pi}{50},\ \frac{3\pi}{50}, \frac{4\pi}{50}\right\}$ rad. We simulate each of these five different systems three times with three different radii each defined by radial factors $r_{factor} = \{0.97,\ 1.00,\ 1.03\}$. This amounts to 15 different

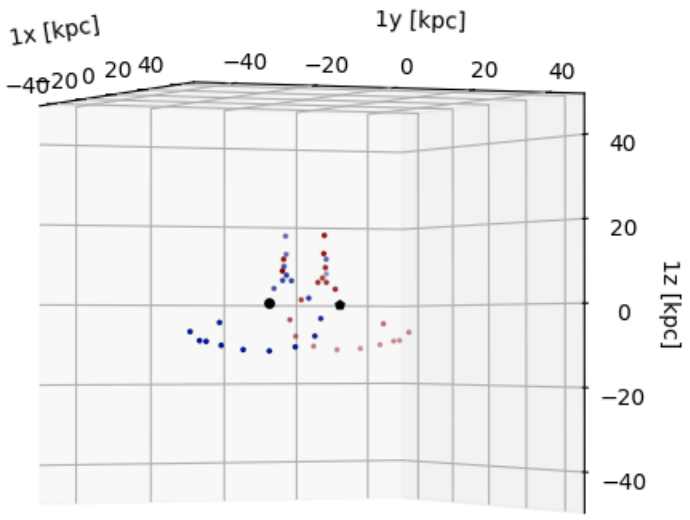

Figure 8: Angled view of a crossing double tail system

simulations.

To allow for correct measurements of distances between structural elements we flatten the rotated 3D plot of the final data as to view it from an angle which makes the system comparable to our view of MRK 231. We rotate the data around the y and z axis respectively and plot the new y' and z' data to create flat images.

Furthermore, to increase clarity when dealing with 3 galaxies we will no longer be plotting the central masses as black particles, but will scale the surface area of each of the markers according to their mass and they will be coloured according to their parent galaxy. This would have detracted from our previous images due to their simplicity, but will enhance our understanding when it comes to the triple galactic interactions. Specifically in regards to visualising the luminosity[4] of the star clusters, which is proportional to their mass (Kuiper, 1938).

These visualisation techniques were used to create the final images such as figure 12.

[4]**Please note**: The particles are point particles (with plummer softening) and their plotted area is proportional to their luminosity and is not proportional to their respective star cluster size.

4 Analysis and Results

Our simulation results include comparisons to original images of MRK 231 and an estimate as to the mass of the third galaxy based on the model which we found to yield the best results.

We refer to the galaxies and the resulting structures as blue, red and green when convenient. This will either be because the galaxy number is no longer applicable (i. e. "the red tail" instead of "the tail consisting primarily of red particles") or because it is easier to differentiate between the galaxies using their colour as opposed to their number (i. e. "the red galaxy" instead of "the second galaxy"). This is done more often when differentiating between the blue (first) and red (second) galaxies, as the initialisation order is not clear unless one consults table 4 and figure 9.

4.1 MRK 231 Simulation

We were able to create structures which were similar to MRK 231 by initialising the third galaxy perpendicular to the xy-plane (i. e. the rotation plane of the two more massive galaxies) with a velocity towards the plane. The initial conditions of this simulation are outlined in table 4. Figure 9 displays where the third galaxy is initialised and figure 10 displays the system 445 Myr after initialisation, up to which point the maximal energy change amounted to $10^{-11)\%}$.

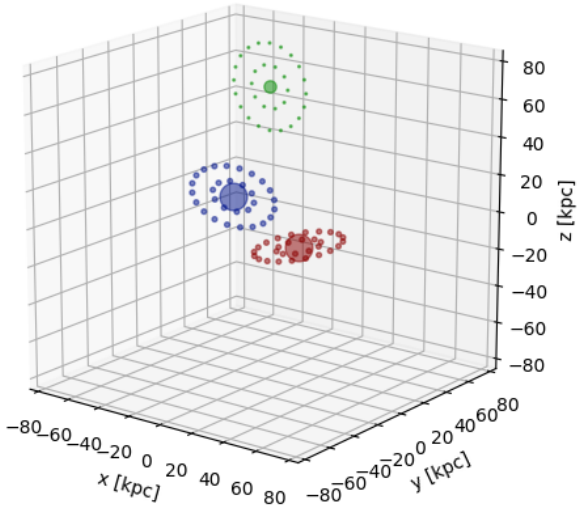

Figure 9: Single simulation initial position of the three galaxies as described in table 4

The angle of protrusion and the dispersion of the third galaxy comes solely from tidal forces as it passes the red galaxy.

Variable	Value	Units
Number of galaxies	3	n.a.
N	[20,10]	n.a.
Outer radius	22.5	kpc
Central mass	10^{11}	$M_\odot$
Galactic mass ratios	[1, 1, 0.2]	n.a.
Gal. 1 velocity factors	[1.32, 1.03]	
Gal. 2 velocity factors	[1.32, 1.03]	**n.a.**
Gal. 3 velocity factors	[0.51, 0.40]	
Rotations around x-Axis	$[-\pi/18, \pi/9, \pi/2]$	
Rotations around y-Axis	$[7\pi/6, 5\pi/6, 0]$	**radians**
Rotations around z-Axis	[0, 0, 0]	
Gal. 1 translation	[−40, −25, 0]	
Gal. 2 translation	[40, 25, 0]	**kpc**
Gal. 3 translation	[12, −12, 75]	
Gal. 1 group velocity	[110, 0, 0]	
Gal. 2 group velocity	[−110, 0, 0]	**pc/Myr**
Gal. 3 group velocity	[0, 0, −170]	

Table 4: Initialisation values of MRK 231 model. See section 3.1.1 for clarification on each variable.

The total mass of the galaxies is set as $2 \cdot 10^{11}\,M_\odot$ as this is a typical mass of a galaxy. This mass was then equally distributed between the central bulge, which is the central particle in our case, and the halo, which are the outer two rings in our construct.

To demonstrate the importance of the third galaxy we remove it from the simulation keeping all other variables the same. Figure 11 shows what the system would look like. We can see that the progression (and thus size) of the red tail is significantly depreciated. The tip of the red tail is approximately 10 kpc further from the origin in comparison to figure 10. We can expect such behaviour specifically because there is very little asymmetry in the system without the third galaxy as the only asymmetric value in the starting conditions is the x-angle rotation which only differs by 10° and according to our observations this seemingly only alters the degree of elevation of the left tail (when viewed from an angle as in figure 11).

To make comparisons to an image of MRK 231 we use the visualisation methods outlined in section 3.5. Figure 12 shows each of the galaxies as separate colours as in previous images, whereas figure 13 shows the system in black and white directly next to a real image of MRK 231 as to provide a clear comparison of the structures which formed.

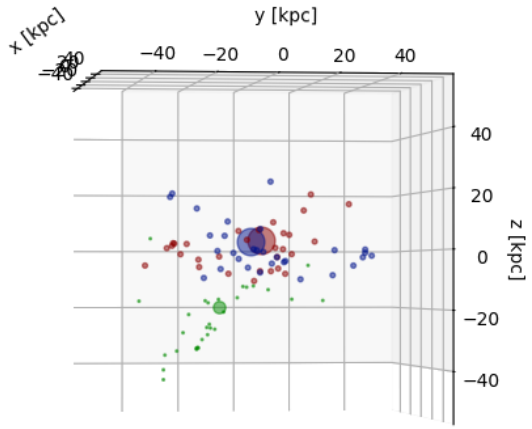

Figure 10: Single simulation plotted at $t = 445\,\text{Myr}$ viewed from the proposed visualisation angle of MRK 231

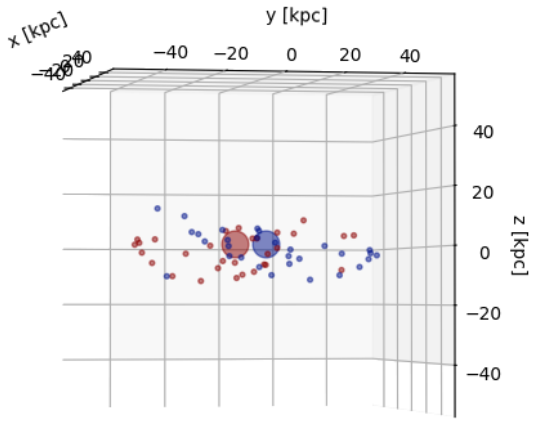

Figure 11: Model without the third galaxy.

As one can see, our model produces a system very similar to MRK 231. Quick measurements of our models results provide us with comparable measurements as seen in table 5. For the measurements made on MRK 231 we use the cosmologically corrected scale[5] of 48.44 kpc/arcmin.

The viewing time and flattening angles were chosen due to visual similarity and are listed in the captions of the respective images.

Value	MRK 231	Model
Span of the two primary tails	61 kpc	70 kpc
Diameter of central area	31 kpc	30 kpc
Length from tip of left tail to central bulge edge	12 kpc	15 kpc
Length from tip of right tail to central bulge edge	18 kpc	24 kpc
Length of tertiary tail to central bulge edge	40 kpc	41 kpc
Angle of protrusion of the tertiary tail	50° - 60°	$\approx 50°$

Table 5: Measurements are taken on figures 2 and 13 respectively. Results for measurements are taken along or are in reference to the y'-axis.

[5]Redshift derived quantities from the NASA/IPAC Extragalactic Database

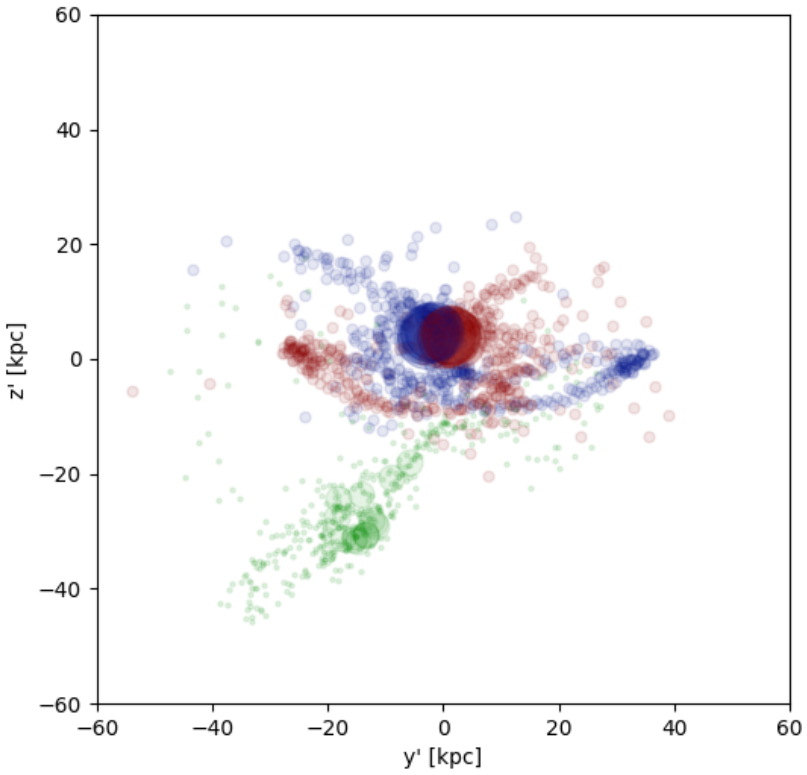

Figure 12: Position of our simulation at $t = 445\,\mathrm{Myr}$ after our starting conditions listed in table 4. Cartesian positions were rotated around the y-axis by $-\pi/90$ radians before being plotted as y' against z'.

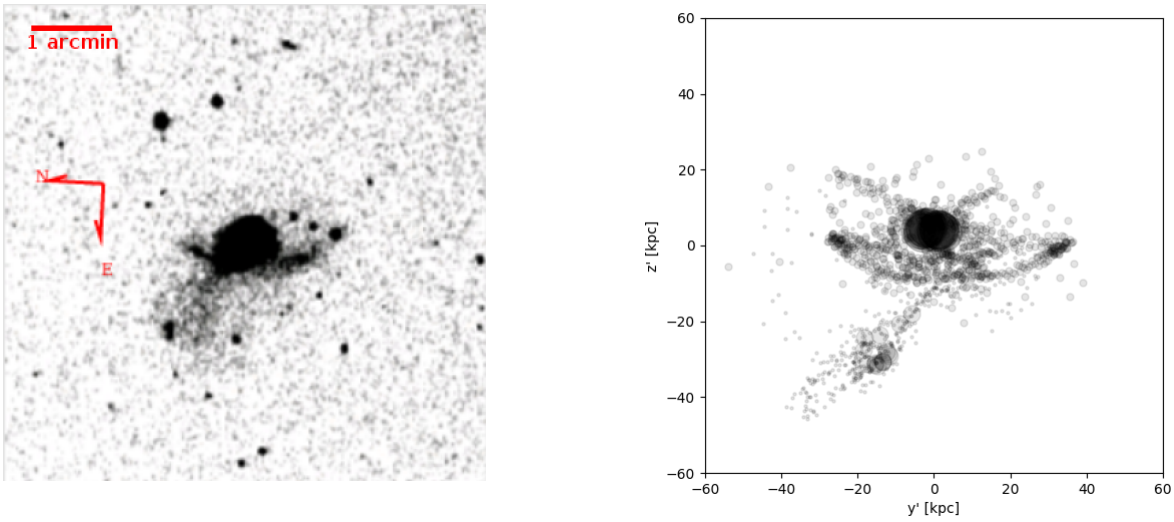

Figure 13: MRK 231 as seen in figure 2 in direct comparison to the black and white merged plot at $t = 445\,\mathrm{Myr}$. The plotted data was rotated around the y-axis by $-\pi/90$ radians before being plotted as y' against z'.

4.2 Model Dependent Mass Prediction

We aim to make a mass prediction of the third galaxy in proportion to the other two galaxies which we assume have very similar mass to one another.

We do this by comparing our final simulation to ones where we alter the mass ratio of the third galaxy and its velocity factors to provide it with the desired stability but leave all other variables equal to those presented in table 4.

We find that the lower bound of the mass ratio is $1/20^{\text{th}}$. The result of which can be seen in figure 14 where the symmetry of the two massive galaxies outweighs the asymmetry provided by the third galaxy leading to a galaxy whose span is too large, and whose red tail is undeniably too long.

We find that the upper bound of mass ratio is $3/10^{\text{ths}}$. This causes the red tail to merge with the central bulge from the merger producing more of a triangular protrusion than a tail, as seen in figure 15.

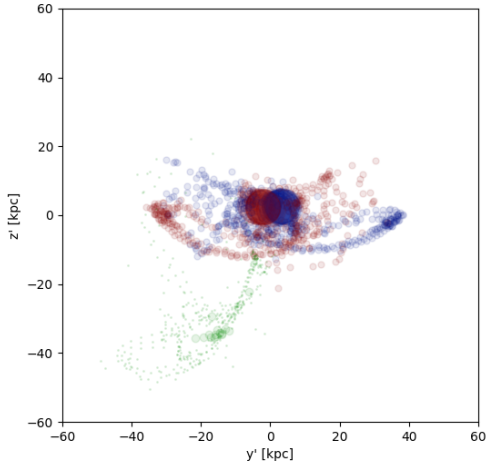

Figure 14: Mass ratio of the third galaxy decreased to 1/20 and velocity ratios corrected to: [0.258, 0.194]

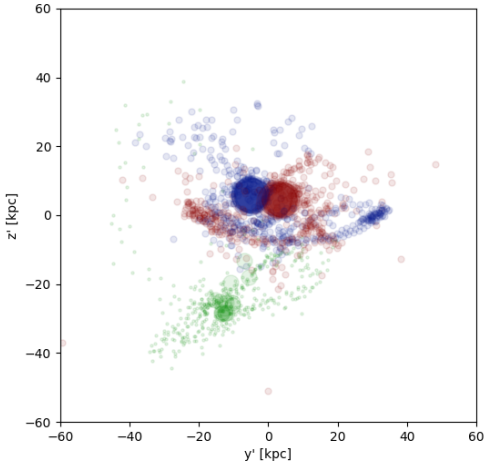

Figure 15: Mass ratio of the third galaxy increased to 3/10 and velocity ratios corrected to: [0.65, 0.5]

As extreme results of mass ratio changes, see figure 11 for a low mass ratio of 0 (since the third galaxy is not present) and figure 16 for a high mass ratio of 1/2. The trends of the red tail extending away from / merging with the bulge seemingly continues up to these extreme mass ratios.

Although it may seem that we have determined the mass ratio (m_r) of the third galaxy to within a range of $\frac{1}{20} < m_r < \frac{6}{20}$ we must mention that there may be other

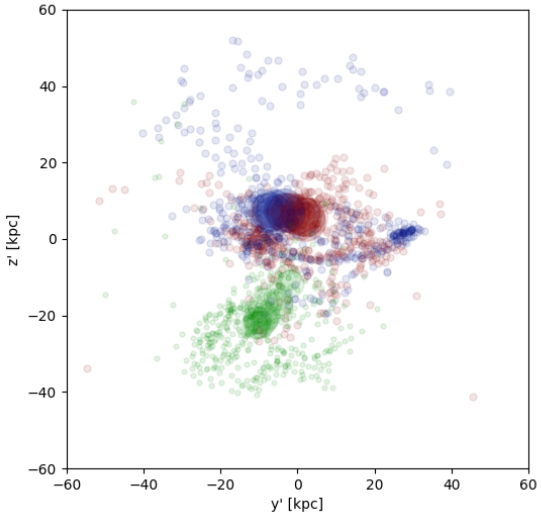

Figure 16: Mass ratio of the third galaxy increased to 1/2 and velocity ratios corrected to: [0.85, 0.655]

times and/or other angles within the respective simulations where these mass ratios produce structures which are much more closely related to MRK 231's structure.

The flux of the equivalent to the "red" tail (data retrieved using IRSA finder chart) is measured at a mean of 1071 ± 5 DN (data numbers), the "blue" tail measured at a mean of 1068 ± 4 DN and the "green" tail is measured at a mean of 1065 ± 4 DN. A measurement of a large background area of the same image (SDSS r: 2003-03-10) produces a flux of 1062 ± 4 DN. When this correction is applied to our base values it produces 9 ± 6 DN for the red tail, 6 ± 5 DN for the blue tail and 3 ± 5 DN for the green tail, which affirms our prediction of the mass ratio being less than half, since the tails themselves are only a fraction of the total mass of each of the larger galaxies.

5 Summary and Outlook

We were able to show that the structure which MRK 231 possesses can be duplicated by modelling its formation as a triple galactic interaction. Our model produced a system which is very similar to images of MRK 231. The largest difference is the two dim "spikes" which protrude from the top of the galaxy. These are relics of our model's simulation method and the assumptions we made. When viewing a single simulation and how it behaves, we observed that close encounters of individual particles in the outer ring with the central masses of the opposite large galaxies disproportionately slingshot these particles towards their final positions in the "spikes" . This would not happen with more sophisticated simulations or in reality as the central bulge of a galaxy is not, and would not be simulated as, a single central point mass.

Our mass prediction of the third interacting galaxy does not contradict the measured flux values. The model dependent mass prediction showed the mass ratio to lie between 0.05 and 0.5 with the best values resulting from a mass ratio of 0.2. As we set the mass of each of the larger galaxies to $2 \cdot 10^{11}\,\mathrm{M}_\odot$ this would mean we predict our third galaxy to have a total mass of $4 \cdot 10^{10}\,\mathrm{M}_\odot$ for our created model.

Further improvements on this research is required, as our model is admittedly over-simplified. However, our model does imply that a third galaxy is not only part of the formation process of MRK 231 but is integral in its formation process to create the asymmetry of the system. We suggest an in depth study of the motion of the tails within MRK 231 as well as more sophisticated and accurate models of the system be made to verify our formation model for MRK 231.

References

Aarseth, S. J. (2003). *Gravitational N-Body Simulations*.

Kuiper, G. P. (1938). "The Empirical Mass-Luminosity Relation." In: 88, p. 472. DOI: 10.1086/143999.

Leighly, Karen M. et al. (2016). In: DOI: 10.3847/0004-637X/829/1/4.

Ma, C. et al. (1998). "The International Celestial Reference Frame as Realized by Very Long Baseline Interferometry". In: *The Astronomical Journal* 116.1, p. 516. URL: http://stacks.iop.org/1538-3881/116/i=1/a=516.

Markarian, B. E. (1967). "Galaxies with an ultraviolet continuum." In: *Astrofizika* 3, pp. 24–38.

Markarian, B. E. et al. (1989). "The First Byurakan Survey - a Catalogue of Galaxies with Ultraviolet Continuum". In: *Soobshcheniya Spetsial'noj Astrofizicheskoj Observatorii* 62, p. 5.

Markaryan, B. E. (1969). "Galaxies with ultraviolet continuum. III". In: *Astrophysics* 5, pp. 286–301. DOI: 10.1007/BF01003911.

Milosavljević, M. and D. Merritt (2003). "The Final Parsec Problem". In: *The Astrophysics of Gravitational Wave Sources*. Ed. by J. M. Centrella. Vol. 686. American Institute of Physics Conference Series, pp. 201–210. DOI: 10.1063/1.1629432. eprint: astro-ph/0212270.

Oh, K. S., D. N. C. Lin, and S. J. Aarseth (1995). "On the tidal disruption of dwarf spheroidal galaxies around the galaxy". In: 442, pp. 142–158. DOI: 10.1086/175429.

Stepanian, J. A. (2005). "The Second Byurakan Survey. General Catalogue". In: 41, pp. 155–368.

Toomre, A. and J. Toomre (1972). "Galactic Bridges and Tails". In: 178, pp. 623–666. DOI: 10.1086/151823.

Yan, Chang-Shuo et al. (2015). "A Probable Milli-parsec Supermassive Binary Black Hole in the Nearest Quasar Mrk 231". In: *The Astrophysical Journal* 809.2, p. 117. URL: http://stacks.iop.org/0004-637X/809/i=2/a=117.

Decleration - Erklärung

I hereby declare that this bachelor thesis is my original work and all sources, resources and quotes which were used have been identified as such.

Hiermit versichere ich, meine Bachelorarbeit selbstständig angefertigt und alle benutzten Quellen, Hilfsmittel und Zitate als solche kenntlich gemacht zu haben.

Micah Ryan Bowles Cologne, Germany, 16^{th} of November 2018